Environmental Research Letters

Supporting Information for

Mangrove diversity loss under sea-level rise triggered by bio-morphodynamic feedbacks and anthropogenic pressures

Danghan Xie[1], Christian Schwarz[1,2], Muriel Z. M. Brückner[1], Maarten G. Kleinhans[1], Dunia H. Urrego[3], Zeng Zhou[4], and Barend van Maanen[1,3]

[1]Faculty of Geosciences, Utrecht University, Utrecht, Netherlands, [2]College of Earth, Ocean, and Environment, University of Delaware, Lewes, DE, USA, [3]College of Life and Environmental Sciences, University of Exeter, Exeter, United Kingdom, [4]College of Harbour, Coastal and Offshore Engineering, Hohai University, Nanjing, China.

Corresponding author: Danghan Xie (d.xie@uu.nl)

Contents of this file

Introduction

This Supporting Information includes ten supplementary figures (Figure S1 to S10), detailed information on the hydro-morphodynamic model (Text S1) and dynamic vegetation model (Test S2), and an overview of model parameter settings (Table S1 and S2).

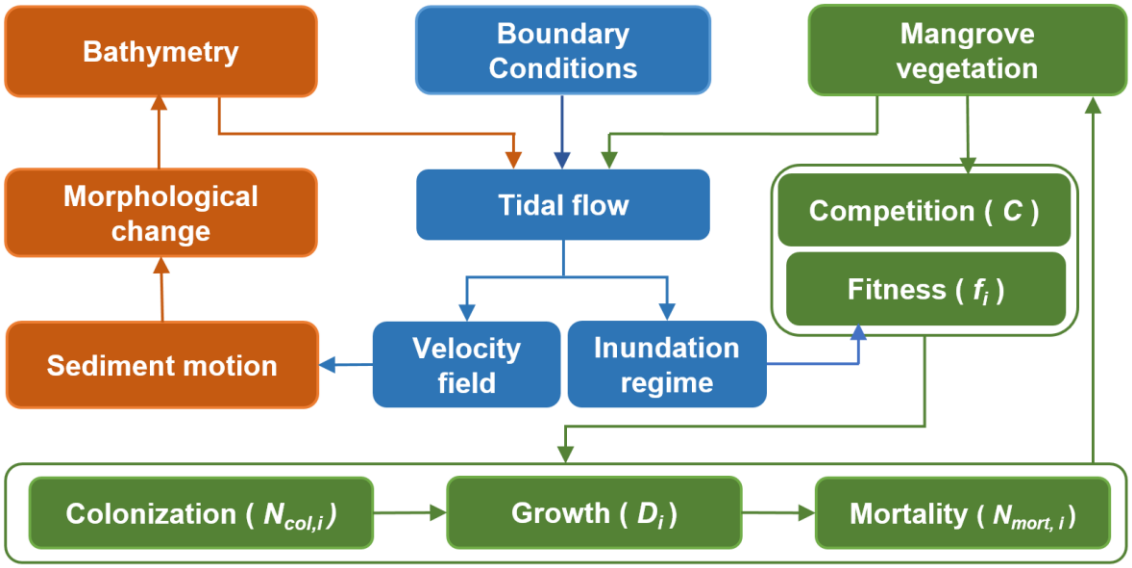

Figure S1. Overview of bio-morphodynamic interactions incorporated into the model. The modelling approach couples a hydro-morphodynamic model and a new dynamic vegetation model so that the interaction between tidal flow, sediment motion, morphological change and mangrove vegetation can be investigated. The vegetation model receives information on the inundation regime from the hydro-morphodynamic model and then regulates the colonization, growth and mortality of species-specific mangrove trees. Information on mangrove vegetation characteristics is in turn exchanged with the hydro-morphodynamic model which then accounts for vegetation effects on tidal flow resistance.

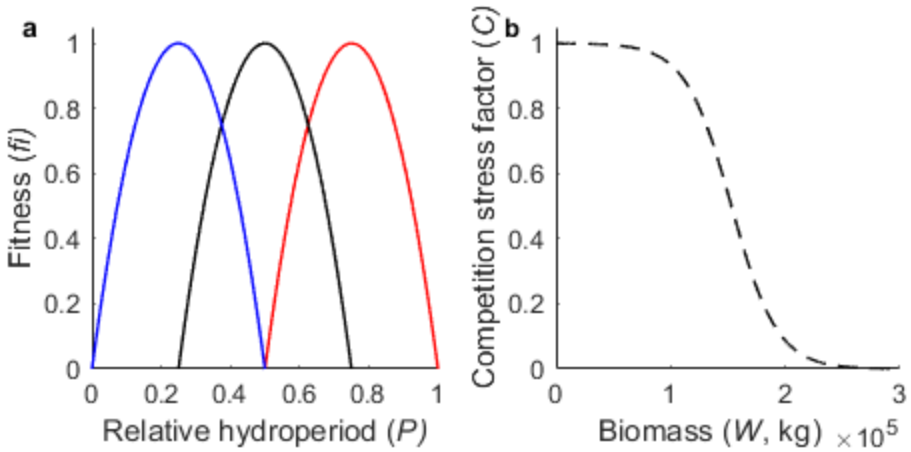

Figure S2. Growth control factors used in the vegetation model. (a) Multi-species fitness functions, characterised by different optimal relative hydroperiods (P = 0 implies never inundated; P = 1 implies permanently inundated). Red, black and blue lines represent the fitness of lower (i.e. *Rhizophora mangle*), middle (i.e. *Avicennia germinans*) and upper mangroves (i.e. *Laguncularia racemosa*), respectively. (b) Competition stress factor representing the influence of vegetation population on growth conditions as neighbouring trees have to share resources.

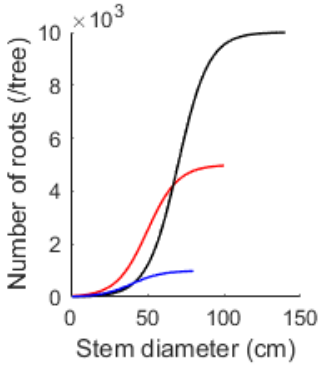

Figure S3. Species-specific number of root elements per tree as a function of mangrove stem diameter. Red, black and blue lines represent lower, middle and upper mangroves. The maximum number of elements per tree varies in order to represent species-specific differences in root structures. Additional simulations are conducted to study the effects of root densities (figure S9).

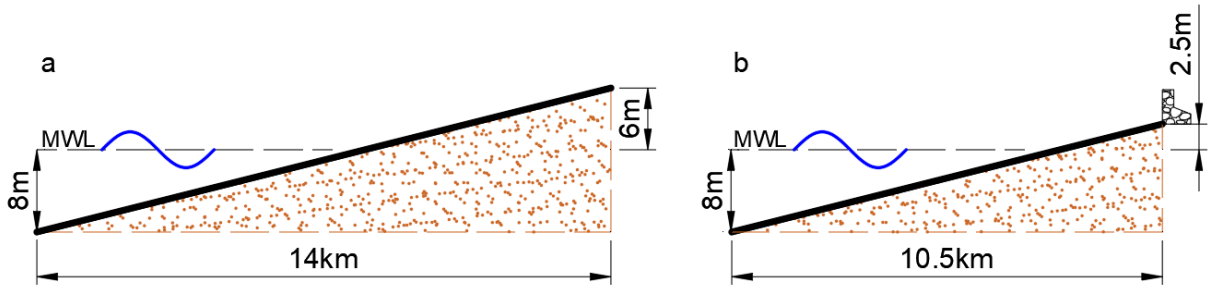

Figure S4. Initial bathymetry and domain settings. a) Domain without tidal barrier, characterised by a 14-km cross-shore distance and a bed elevation of 6 m at the landward boundary, such that sea-level rise causes flooding of previously dry areas and a dynamic wetting/drying boundary exists. b) Domain with tidal barrier, characterised by a 10.5-km cross-shore distance and a bed elevation of 2.5 m at the landward boundary, which is equal to the high water level at the beginning of the simulation. This means that the entire domain gets submerged and the landward side acts as a closed boundary similar to a non-permeable dike or seawall (Zhou et al., 2016).

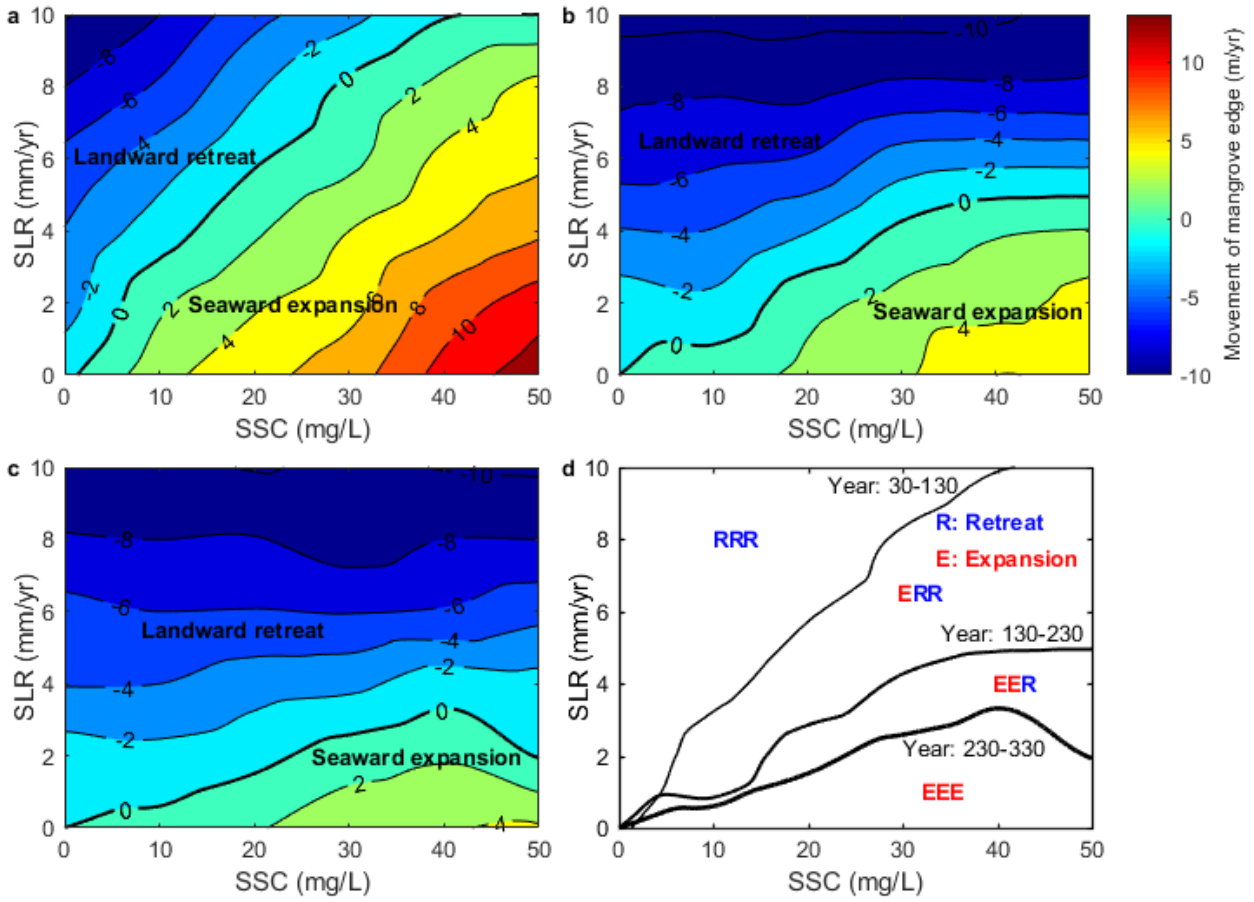

Figure S5. Temporal variation in the movement of the seaward forest edge under different combinations of external suspended sediment concentration (SSC) and sea-level rise rate (SLR) without barrier. (a) Movement of the seaward forest edge in the first 100 years (i.e., from year 30 to year 130) shows that more than half of the simulated SSC-SLR combinations result in initial mangrove expansion. (b) Mangrove movement in the second 100 years (i.e., from year 130 to year 230) reveals that a shift from expansion to retreat can emerge, highlighting dynamic forest behaviour and the effects of prolonged sea-level rise. (c) Mangrove movement in the third 100 years (i.e., from year 230 to year 330) indicates that persistent mangrove expansion is only possible under low sea-level rise. (d) Overview of mangrove movement over the different 100-year periods, suggesting that shifts from expansion to retreat are possible for a broad range of SSC-SLR combinations. The black lines in d represent a stable seaward forest edge when evaluated over each distinct period and correspond to the 0 m/yr contour lines in a, b and c.

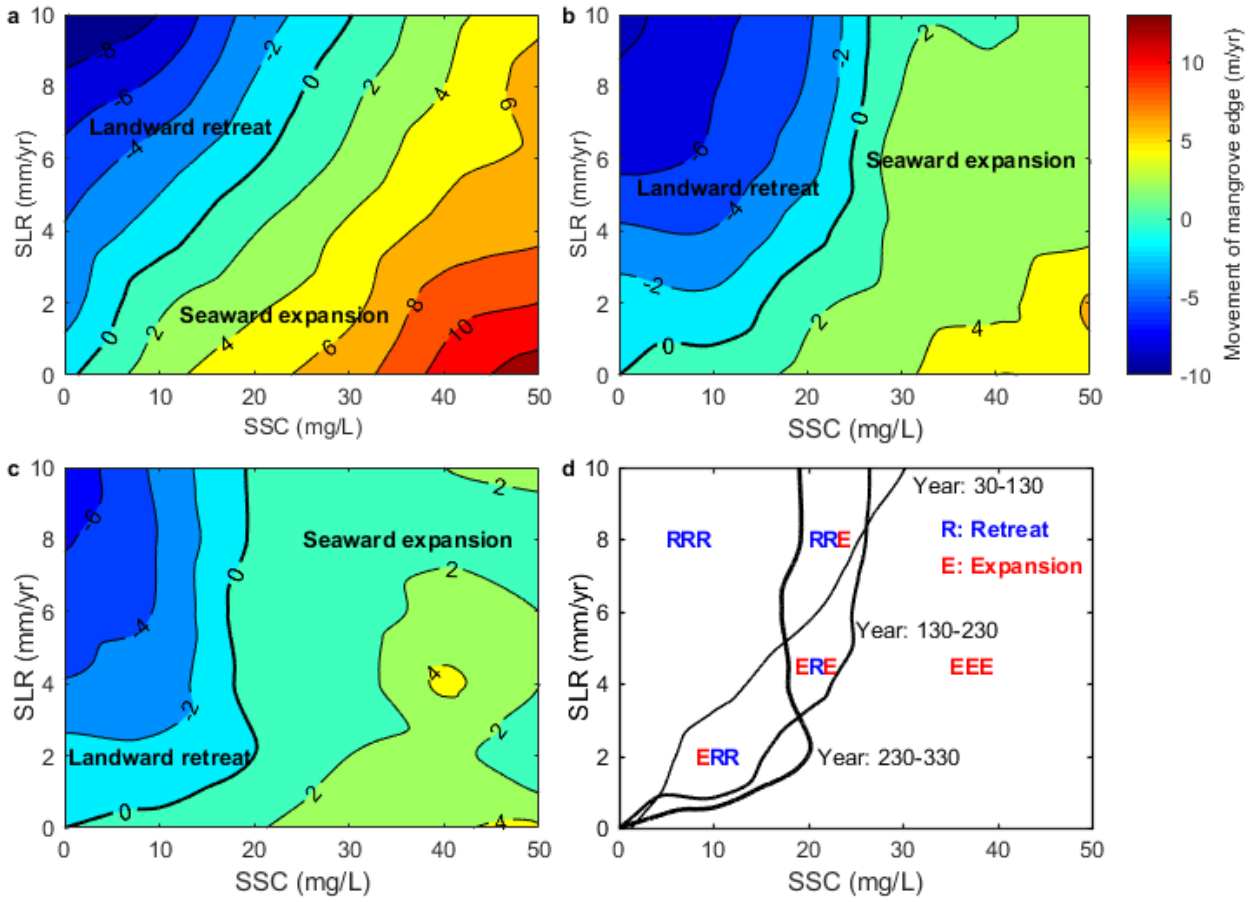

Figure S6. Temporal variation in the movement of the seaward forest edge under different combinations of external suspended sediment concentration (SSC) and sea-level rise rate (SLR) with barrier. (a) Movement of the seaward forest edge in the first 100 years (i.e., from year 30 to year 130) shows that the majority of simulated SSC-SLR combinations drives initial mangrove expansion. (b) Mangrove movement in the second 100 years (i.e., from year 130 to year 230) indicates that mangrove expansion is generally maintained, although the rate of expansion reduces. (c) Mangrove movement in the third 100 years (i.e., from year 230 to year 330) highlights that shifts from mangrove retreat to expansion are also possible. (d) Overview of mangrove movement over the different 100-year periods, highlighting that the presence of a barrier reduces the parameter space that results in shifts from expansion to retreat, or vice versa. The black lines in d represent a stable seaward forest edge when evaluated over each distinct period and correspond to the 0 m/yr contour lines in a, b and c.

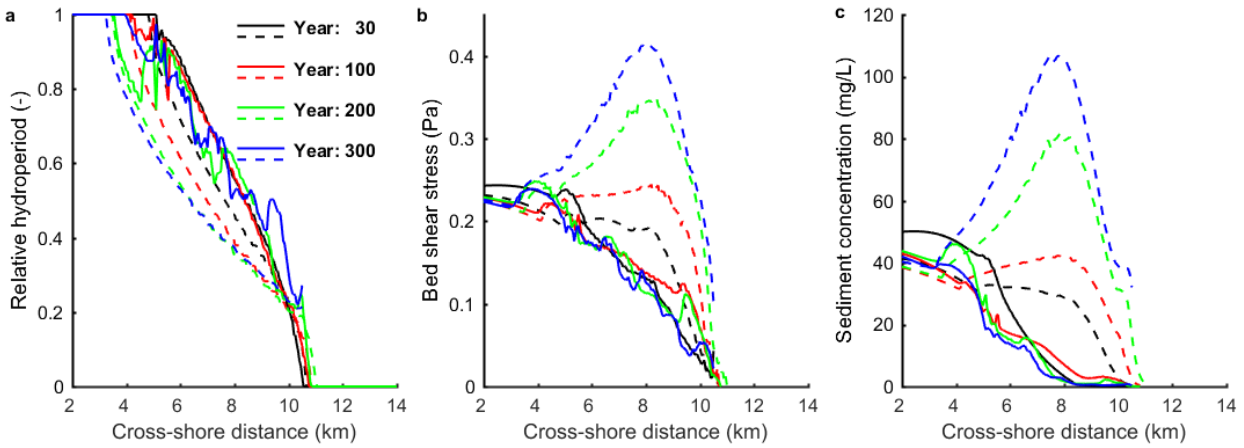

Figure S7. Cross-shore trends in relative hydroperiod, bed shear stress and sediment concentration obtained after 30, 100, 200 and 300 years of profile and forest development with original root settings. Results are extracted from a simulation driven with an external sediment supply of 50 mg/L and sea-level rise rate of 2 mm/yr (see first column of figure 4 in the main paper). Solid lines represent the corresponding trends when the effects of vegetation on flow resistance are included, while the dashed lines represent the trends without vegetation impacts (using the same bathymetry). a-c indicate that vegetation is responsible for increasing inundation periods, weakening tidal currents and reducing suspended sediment concentration levels. The delivery of sediment to the upper part of the forest becomes increasingly limited as mangroves are expanding under these high external sediment supply conditions.

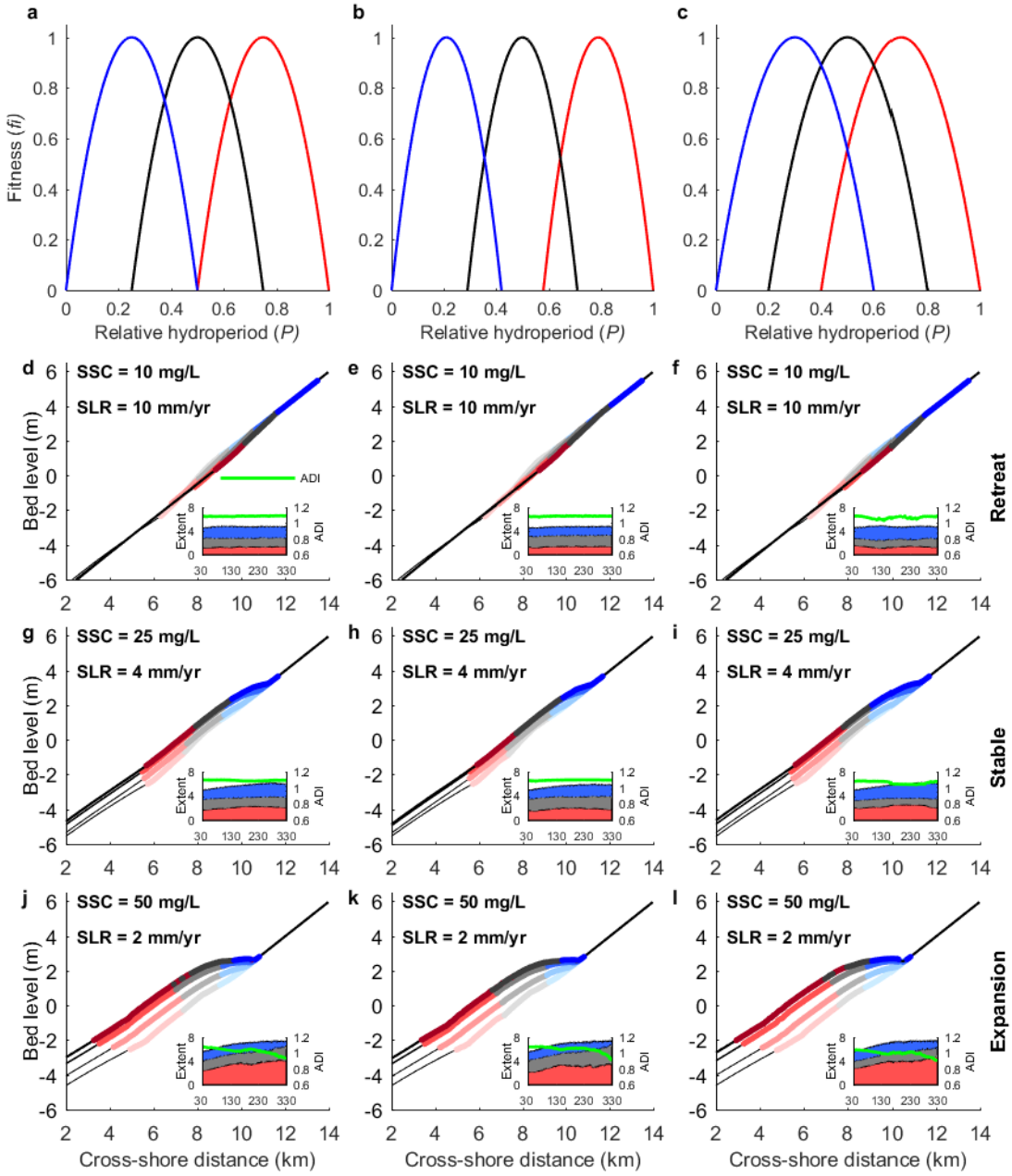

Figure S8. Distinct forest behaviours in response to different combinations of sea-level rise and sediment supply under different species distribution criteria (first column: original settings; second column: narrower species distributions; third column: wider species distributions). (a-c) Fitness functions for the different species distribution criteria. Red, black and blue lines indicate the fitness of lower, middle and upper mangroves, respectively. (d-f) Landward retreat of mangrove species. (g-i) Temporal stability of the seaward forest edge. (j-l) Seaward expansion of the mangrove forest. Evolution of the coastal profile and mangrove forest are shown after 30, 100, 200 and 300 years.

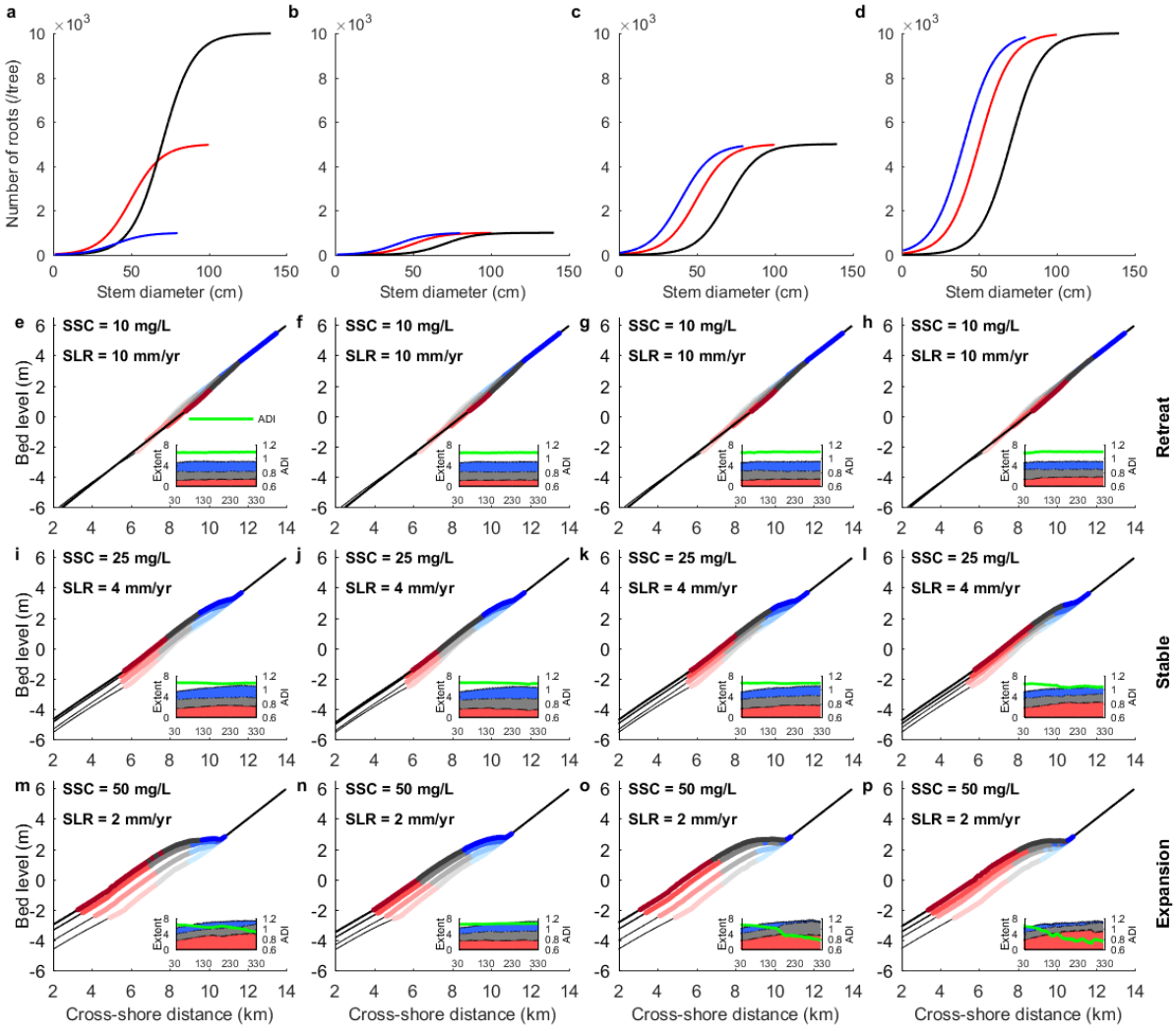

Figure S9. Distinct forest behaviours in response to different combinations of sea-level rise and sediment supply under different root densities (first column: original settings; second to fourth columns: maximum number of root elements per tree is species-independent and set to 1000, 5000 and 10000, respectively). (a-d) Species-specific number of root elements per tree as a function of mangrove stem diameter for the different root density settings. Red, black and blue lines indicate the number of root elements of lower, middle and upper mangroves, respectively. (e-h) Landward retreat of mangrove species. (i-l) Temporal stability of the seaward forest edge. (m-p) Seaward expansion of the mangrove forest. Evolution of the coastal profile and mangrove forest are shown after 30, 100, 200 and 300 years.

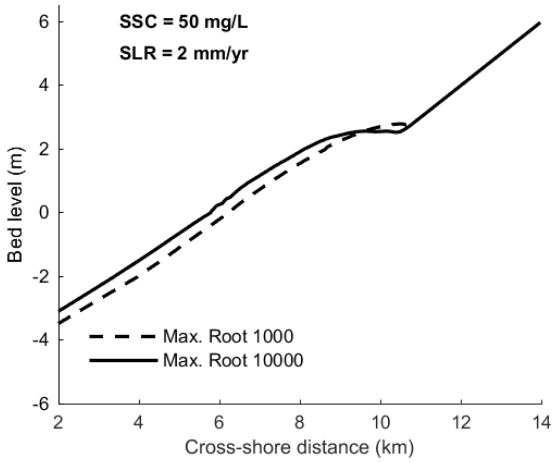

Figure S10. Comparison of coastal profiles after 300 years between low and high root densities. Maximum number of root elements per tree is species-independent and set to 1000 and 10000. Dense roots contribute to profile progradation while less roots allow for enhanced sediment delivery to the more landward region and a slightly larger accretion in the upper part of the mangrove forest.

Text S1. Hydro-morphodynamic model description

The Delft3D hydro-morphodynamic model computes tidal flow, sediment transport and related bathymetric changes. A detailed description of the model can be found elsewhere (Lesser et al., 2004; Zhou et al., 2016); here we provide a short overview of the governing equations. Water level and flow velocity are obtained by solving the basic conservation of mass and momentum equations as follows:

$$\frac{\partial \eta}{\partial t} + \frac{\partial (hu)}{\partial x} = 0 \tag{1}$$

$$\frac{\partial u}{\partial t} + u\frac{\partial u}{\partial x} = -g\frac{\partial \eta}{\partial x} + \nu\frac{\partial^2 u}{\partial x^2} - g\frac{u|u|}{C^2 h} + M_x \tag{2}$$

where η is the water level (m) with respect to datum (e.g. mean sea level); h is the water depth (m); u is the depth-averaged flow velocity (m/s); $g = 9.81$ m/s^2 is the gravitational acceleration; $\nu = 10$ m^2/s is the horizontal eddy viscosity coefficient; C is the Chézy friction coefficient (m$^{1/2}$/s) and M_x is an extra momentum term linked to vegetation effects. The presence of vegetation is incorporated by including additional hydraulic resistance, which is considered through calculation of the Chézy friction coefficient and the additional resistance term ($M_x = -\frac{\lambda}{2}u^2$). Both λ and C are derived from vegetation characteristics (diameter, height, density) and water depth (Brückner et al., 2019):

$$\lambda = \begin{cases} C_D n \frac{h_v}{h}\frac{C_b^2}{C^2} & , if \;\; h \geq h_v \\ C_D n & , if \; h < h_v \end{cases} \tag{3}$$

$$C = \begin{cases} C_b + \frac{\sqrt{g}}{\kappa}\ln\left(\frac{h}{h_v}\right)\sqrt{1 + \frac{C_D n h_v C_b^2}{2g}} & , if \; h \geq h_v \\ C_b & , if \; h < h_v \end{cases} \tag{4}$$

where C_b is the non-vegetated Chézy coefficient, set to 65 (m$^{1/2}$/s); $\kappa = 0.41$ is the Von Kármán constant; h_v is the height of vegetation objects (stems or roots) (m); C_D is the drag coefficient and $n = mD$ where m is the number of vegetation objects per square metre and D is the diameter of this object. If vegetation biomass, such as roots and trunks with different sizes co-exist in one grid cell, C and λ are calculated separately for each vegetation object and averaged with the specific fraction coverage of each vegetation object (Brückner et al., 2019).

Regarding sediment transport, we consider pure cohesive sediment as mangroves commonly thrive in muddy environments. Deposition ($Q_{mud,d}, kg \cdot m^{-2}s^{-1}$) and erosion fluxes ($Q_{mud,e}, kg \cdot m^{-2}s^{-1}$) are estimated through the widely-adopted Partheniades-Krone formulations as follows:

$$Q_{mud,d} = \begin{cases} \omega_s c\left(1 - \frac{\tau_c}{\tau_{cr,d}}\right), if \; \tau_c < \tau_{cr,d} \\ 0 \qquad\qquad , if \; \tau_c \geq \tau_{cr,d} \end{cases} \tag{5}$$

$$Q_{mud,e} = \begin{cases} M_e \left(\frac{\tau_c}{\tau_{cr,e}} - 1 \right), if\ \tau_c > \tau_{cr,e} \\ 0 \qquad\qquad\qquad\quad , if\ \tau_c \leq \tau_{cr,e} \end{cases} \tag{6}$$

where $\omega_s = 5 \times 10^{-4}$ m/s is the settling velocity, c is the depth-averaged sediment concentration (kg/m^3), $\tau_c = \rho g u^2 / C^2$ is the tide-induced bottom bed shear stress (Pa), $\tau_{cr,d} = 1000$ Pa and $\tau_{cr,e} = 0.2$ Pa are the critical shear stresses for deposition and erosion, respectively. $M_e = 5 \times 10^{-5}$ kg/m^2/s is the erosion parameter. These parameter settings are representative for mud dominated environments (Zhou et al., 2016). The transport of suspended sediment is calculated according to the advection-diffusion equation and this allows us to model the transport of sediment between different regions of the mangrove forest:

$$\frac{\partial (ch)}{\partial t} + \frac{\partial (uch)}{\partial x} = Q_{mud,e} - Q_{mud,d} \tag{7}$$

Bed level changes are then calculated following the mass conservation equation of cohesive sediment:

$$(1 - \varepsilon_p) \frac{\partial z_b}{\partial t} = \frac{1}{\rho_s} (Q_{mud,d} - Q_{mud,e}) \tag{8}$$

where ε_p is the bed porosity, set to 0.4; z_b is the bed profile elevation (m) and ρ_s is the density of sediment (kg/m^3), set to 2650 kg/m^3. A morphological acceleration factor (Brückner et al., 2019; Lesser et al., 2004) was used, meaning that the erosion and deposition fluxes computed during a hydrodynamic time step are enlarged by this factor (set to 30 in this study based on earlier tests). This approach is commonly used in morphodynamic modelling and allow us to accomplish long-term simulations.

Text S2. Dynamic vegetation model description

To simulate the colonization, growth and mortality of mangroves, a dynamic vegetation model was developed based on earlier work on mangrove modelling (van Maanen et al., 2015). The major advancement is the ability to simulate the dynamics of mangrove assemblages with multiple species occupying the lower, middle and upper intertidal area. In this study, we represent the physical characteristics of mangroves in each zone by a characteristic species. We therefore selected three species, namely *Rhizophora mangle, Avicennia germinans* and *Laguncularia racemosa*, to represent lower, middle and upper intertidal mangroves, respectively. These species commonly co-exist in intertidal habitats and are known to thrive at different elevations (Chapman, 1976; Duke et al., 1998; Lugo and Snedaker, 1974). Furthermore, detailed information on the growth parameters for these species is available (Berger and Hildenbrandt, 2000; Chen and Twilley, 1998).

Colonization by mangroves occurs each year and is dependent on suitable inundation regimes. We therefore used inundation based fitness functions to define species-specific growth conditions (D'Alpaos and Marani, 2016; van Maanen et al., 2015):

$$f_i = a_i \cdot P^2 + b_i \cdot P + c_i \quad (9)$$

where P is the relative hydroperiod calculated as the proportion of time that the bed is inundated per tidal cycle and a_i, b_i and c_i are species-specific constants. The fitness functions suggest that each species has a specific hydroperiod for which growth is optimal while growth conditions diminish when mangroves are inundated for either longer or shorter periods (van Maanen et al., 2015). For the sake of comparability, all species were given an equal maximum fitness (i.e., $f_{max,1}$ = $f_{max,2}$= $f_{max,3}$= 1) and the shape of each fitness function is symmetric and equal as well (figure S2(a)). These functions then control colonization processes: mangrove trees of a specific species can only colonize when its fitness exceeds zero ($f_i > 0$). If that is the case, mangroves establish with an initial mangrove density of 30 individuals per 100 m^2 which is assumed to be the maximum density and an initial stem diameter of 1.37 cm (Berger and Hildenbrandt, 2000; van Maanen et al., 2015). If inundation conditions allow co-existence of multiple species, then the number of individuals per species able to colonize is weighted by its fitness level (f_i):

$$N_{col,i} = N_{col,max} \cdot \frac{f_i}{\sum_{i=1}^{n} f_i} \quad (10)$$

where $N_{col,i}$ is the number of colonizing trees of species i and $N_{col,max}$ is the maximum number of trees that can be added to one grid cell, which is equal to the initial mangrove density multiplied by grid size.

Mangrove growth is implemented by increasing both stem diameter and tree height over time, and is described as (Berger and Hildenbrandt, 2000; Chen and Twilley, 1998; van Maanen et al., 2015) :

$$\frac{dD_i}{dt} = \frac{G_i D_i \left(1 - \frac{D_i H_i}{D_{max,i} H_{max,i}}\right)}{(274 + 3b_{2i} D_i - 4b_{3i} D_i^2)} \cdot f_i \cdot C \quad (11)$$

$$H_i = 137 + b_{2i} D_i - b_{3i} D_i^2 \quad (12)$$

where D_i is the stem diameter (cm) and H_i is the height (cm) for the *i*th tree species, and t is time (years). $D_{max,i}$ and $H_{max,i}$ are the species-specific maximum stem diameter and tree height, respectively. G_i, b_{2i} and b_{3i} are growth parameters. The growth function considers species-specific fitness which is added as an additional factor and modifies mangrove growth. A reduction in growth rate takes place when inundation conditions are sub-optimal reflected by a fitness smaller than 1 ($f_i < 1$). Tree growth is further affected by limitations in available resources, which is incorporated by adding a competition stress factor *C* (van Maanen et al., 2015):

$$C = \frac{1}{1 + \exp[d(W_{0.5} - W)]} \quad (13)$$

where d is a constant controlling the overall shape of the function, and is set to -0.00005. W is the actual above-ground biomass (kg) that is present in a grid cell and $W_{0.5}$ is a characteristic biomass (kg) defined as the value of W for which C = 0.5 (figure S2(b)). In order to compute W, we consider the total number of trees per grid cell and the weight of each single tree, derived through species-specific allometric equation (Komiyama et al., 2008):

$$W = \sum_{i}^{n} \sum_{j}^{m} \alpha_i \cdot D_{i,j}^{\beta_i} \quad (14)$$

where n is the total number of mangrove species and *m* is the total number of trees per species *i*. α_i and β_i are species-specific constants. To derive $W_{0.5}$, the 'zone of influence' concept (Berger and Hildenbrandt, 2000) is applied which considers a circular zone around each mangrove tree, with radius R, in which the tree exploits resources (Berger and Hildenbrandt, 2000):

$$R = 10\sqrt{rbh} \quad (15)$$

where rbh is the stem radius (m). As there may be more than one species in a grid cell, we adopted an average biomass to calculate $W_{0.5}$:

$$W_{0.5} = \frac{1}{n} \sum_{i=1}^{n} \left(\frac{A_{cell}}{(2 \cdot R_i)^2} \cdot W_{max,i} \right) \quad (16)$$

where A_{cell} is the grid cell surface area (m^2) and $W_{max,i}$ is the maximum tree weight (kg) of species *i*. The above equation provides a characteristic biomass per grid cell under the condition that the zones of influence around each tree are not overlapping (i.e. limited competition for resources) (van Maanen et al., 2015). As A_{cell} equals to 2500 m^2 in our study, application of Equation (16) leads to $W_{0.5}$ being set to 1.53×10^5 kg for each grid cell (figure S2(b); C = 0.5, if $W = W_{0.5}$).

Mangrove mortality occurs due to prolonged periods of suppressed growth (Berger and Hildenbrandt, 2000). At the end of every year, the growth condition of each tree is therefore evaluated by calculating the yearly averaged value of $f_i \cdot C$ which controls the growth rate as defined by Equation (11). Trees die when the growth is less than 50% of the growth under optimal conditions (i.e., $f_i \cdot C < 0.5$) for 5 consecutive years (van Maanen et al., 2015). This drives a self-thinning process as the density of trees decreases, leading to an overall biomass reduction, until the growth condition of remaining trees is no longer suppressed, and the values of $f_i \cdot C$ thus equal or exceed 0.5. Small trees are assumed to be more fragile and die first. If tree mortality occurs among multiple species co-existing in a grid cell, then the removal of trees is weighted by the relative fitness factors, such that a lower fitness results in a higher mortality:

$$N_{mort,i} = \frac{N_{mort,tot}}{f_i \cdot \sum_i^n \frac{1}{f_i}} \tag{17}$$

where $N_{mort,i}$ is the number of trees of species *i* and $N_{mort,tot}$ is the total number of trees that need to be removed. On the other hand, if growth conditions are favourable (i.e., $f_i \cdot C > 0.5$) and the maximum density is not reached, young mangrove trees are added such that a single grid cell can contain trees of different sizes (van Maanen et al., 2015).

Apart from tree trunks, mangrove aerial roots are known to provide significant flow resistance (Asbridge et al., 2016; Krauss et al., 2014; Mazda et al., 1997; van Maanen et al., 2015), hence a description of mangrove root systems is required. Aerial root structures vary greatly among species (Tomlinson, 2016). For example, *Rhizophora mangle* trees have prop roots arching from their trunks to the ground, while *Avicennia germinans* trees have pencil-like pneumatophores extending upward from underground cable roots. The root system of *Laguncularia racemosa* trees is less extensive and may include limited pneumatophores. As the hydro-morphodynamic model only allows for inclusion of cylindrical objects, we simplified the shape of roots to cylinders characterized by a fixed diameter and height. The number of root elements is related to stem diameter according to a sigmoid function and increases with tree size (figure S3) (van Maanen et al., 2015):

$$N_{roots,i} = m_i \cdot \frac{1}{1 + exp\left[f\left(\frac{D_{max,i}}{2} - D\right)\right]} \tag{18}$$

where m_i is the maximum number of root elements for one single tree of species *i* and $f = 0.1$ is a constant describing the rate of increase. The maximum number of root elements per tree is species-specific in order to represent differences in root structures. The sensitivity of mangrove forest behaviour to different root densities has been investigated (figure S9).

Table S1. Hydro-morphodynamic model parameter settings

Category	Parameter	Value/Description	Unit
Time reference	Hydrodynamic time step	0.5	min
	Morphological acceleration factor	30	-
	Simulated period	330	years
Domain	Initial slope	1/1000	m/m
	Domain size (x × y) without barrier	14000 × 14 (-8 to 6)	m
	Domain size (x × y) with barrier	10500 × 10.5 (-8 to 2.5)	m
	Grid size (N × M)	50 × 50	m
Bottom roughness	Chézy value at bare substrate	65	$m^{1/2}/s$
Boundary condition	Tidal amplitude	2.5	m
Sediment	Critical bed shear stress for erosion	0.2	N/m^2
	Critical bed shear stress for deposition	1000	N/m^2
	Erosion parameter	5×10^{-5}	$kg/m^2/s$

Table S2. Dynamic vegetation model parameter settings. Values for maximum root number and fitness function constants reported here are the original settings. Sensitivity to these parameter settings has been investigated to explore the influence of species distribution criteria (figure S8) and root densities (figure S9) on mangrove assemblage behaviour.

Category	Parameter	Lower-mangroves	Middle-mangroves	Upper-mangroves	Unit	Source
		R. mangle	***A. germinans***	***L. racemosa***		
Vegetation parameters	Initial stem diameter	1.37	1.37	1.37	cm	(Berger and Hildenbrandt, 2000; van Maanen et al., 2015)
	Maximum root number	5000	10000	1000	-	(Tomlinson, 2016; van Maanen et al., 2015)
	Root diameter	1	1	1	cm	(van Maanen et al., 2015)
	Root height	15	15	15	cm	(van Maanen et al., 2015)
	Drag coefficient of vegetation	1	1	1	-	(Brückner et al., 2019)
Growth parameters	Maximum stem diameter	100	140	80	cm	(Berger and Hildenbrandt, 2000; Chen and Twilley, 1998)
	Maximum tree height	4000	3500	3000	cm	(Berger and Hildenbrandt, 2000; Chen and Twilley, 1998)
	Growth constant G	267	162	243	cm/yr	(Berger and Hildenbrandt, 2000; Chen and Twilley, 1998)
	Growth constant b_2	77.26	48.04	71.58	-	(Berger and Hildenbrandt, 2000; Chen and Twilley, 1998)
	Growth constant b_3	0.396	0.172	0.447	-	(Berger and Hildenbrandt,

					2000; Chen and Twilley, 1998)
	Fitness function constant *a*	-16	-16	-16	-	
	Fitness function constant *b*	24	16	8	-	
	Fitness function constant *c*	-8	-3	0	-	
	Biomass constant α	0.178	0.14	0.102	-	(Komiyama et al., 2008)
	Biomass constant β	2.47	2.4	2.5	-	(Komiyama et al., 2008)

References

Asbridge, E., Lucas, R., Ticehurst, C., and Bunting, P. (2016), Mangrove response to environmental change in Australia's Gulf of Carpentaria, *Ecol Evol*, *6*(11), 3523-3539.

Berger, U., and Hildenbrandt, H. (2000), A new approach to spatially explicit modelling of forest dynamics: spacing, ageing and neighbourhood competition of mangrove trees, *Ecological Modelling*, *132*, 287-302.

Brückner, M. Z. M., Schwarz, C., van Dijk, W. M., van Oorschot, M., Douma, H., and Kleinhans, M. G. (2019), Salt Marsh Establishment and Eco-Engineering Effects in Dynamic Estuaries Determined by Species Growth and Mortality, *Journal of Geophysical Research: Earth Surface*, *124*(12), 2962-2986.

Chapman, V. J. (1976), *Mangrove vegetation*, J. Cramer, Vaduz.

Chen, R., and Twilley, R. R. (1998), A gap dynamic model of mangrove forest development along gradients of soil salinity and nutrient resources, *Journal of Ecology*, *86*, 37-51.

D'Alpaos, A., and Marani, M. (2016), Reading the signatures of biologic–geomorphic feedbacks in salt-marsh landscapes, *Advances in Water Resources*, *93*, 265-275.

Duke, N. C., Ball, M., and Ellison, J. (1998), Factors influencing biodiversity and distributional gradients in mangroves, *Global Ecology and Biogeography Letters*, *7*, 27-47.

Komiyama, A., Ong, J. E., and Poungparn, S. (2008), Allometry, biomass, and productivity of mangrove forests: A review, *Aquatic Botany*, *89*(2), 128-137.

Krauss, K. W., McKee, K. L., Lovelock, C. E., Cahoon, D. R., Saintilan, N., Reef, R., and Chen, L. (2014), How mangrove forests adjust to rising sea level, *New Phytol*, *202*(1), 19-34.

Lesser, G. R., Roelvink, J. A., van Kester, J. A. T. M., and Stelling, G. S. (2004), Development and validation of a three-dimensional morphological model, *Coastal Engineering*, *51*(8-9), 883-915.

Lugo, A. E., and Snedaker, S. C. (1974), The ecology of mangroves, *Annual Review of Ecology and Systematics*, *5*, 39-64.

Mazda, Y., Wolanski, E., King, B., Sase, A., Ohtsuka, D., and Magi, M. (1997), Drag force due to vegetation in mangrove swamps, *Mangroves and Salt Marshes*, *1*(3), 193-199.

Tomlinson, P. B. (2016), *The Botany of Mangroves*, 2 ed., Cambridge University Press, Cambridge.

van Maanen, B., Coco, G., and Bryan, K. R. (2015), On the ecogeomorphological feedbacks that control tidal channel network evolution in a sandy mangrove setting, *Proc Math Phys Eng Sci*, *471*(2180), 20150115.

Zhou, Z., Ye, Q., and Coco, G. (2016), A one-dimensional biomorphodynamic model of tidal flats: Sediment sorting, marsh distribution, and carbon accumulation under sea level rise, *Advances in Water Resources*, *93*, 288-302.